

The effect of ITER-like wall on runaway electron generation in JET

G. Papp^{1,2}, T. Fülöp¹, T. Fehér³, P. C. de Vries⁴, V. Riccardo⁵,
C. Reux⁶, M. Lehnen⁷, V. Kiptily⁵, V. V. Plyusnin⁸, B. Alper⁵
and JET EFDA contributors⁹

JET-EFDA Culham Science Centre, OX15 3DB, Abingdon, UK

¹Department of Applied Physics, Nuclear Engineering, Chalmers University of Technology and Euratom-VR Association, SE-41296 Göteborg, Sweden

²Department of Nuclear Techniques, Budapest University of Technology and Economics, Association EURATOM, H-1111 Budapest, Hungary

³Max Planck Institute for Plasma Physics, EURATOM Association, Boltzmannstr. 2, 85748 Garching, Germany

⁴FOM institute DIFFER, Association EURATOM-FOM, PO Box 120, Nieuwegein, Netherlands

⁵CCFE/EURATOM Association, Culham Science Centre, Abingdon, OX14 3DB, UK

⁶Ecole Polytechnique, CNRS, 91128 Palaiseau Cedex, France

⁷Institut für Energie- und Klimaforschung-IEK-4, Forschungszentrum Jülich GmbH, EURATOM Association, 52425 Jülich, Germany

⁸Instituto de Plasmas e Fusão Nuclear/IST, Associacao EURATOM-IST, Av. Rovisco Pais, 1049-001 Lisbon, Portugal

⁹See the Appendix of F. Romanelli et al., Proceedings of the 24th IAEA Fusion Energy Conference 2012, San Diego, US

E-mail: papp@chalmers.se

Abstract.

This paper investigates the effect of the ITER-like wall (ILW) on runaway electron (RE) generation through a comparative study of similar slow argon injection JET disruptions, performed with different wall materials. In the carbon wall case, a runaway electron plateau is observed, while in the ITER-like wall case, the current quench is slower and the runaway current is negligibly small. The aim of the paper is to shed light on the reason for these differences by detailed numerical modelling to study which factors affected the RE formation. The post-disruption current profile is calculated by a one-dimensional model of electric field, temperature and runaway current taking into account the impurity injection. Scans of various impurity contents are performed and agreement with the experimental scenarios is obtained for reasonable argon- and wall impurity contents. Our modelling shows that the reason for the changed RE dynamics is a complex, combined effect of the differences in plasma parameter profiles, the radiation characteristics of beryllium and carbon, and the difference of the injected argon amount. These together lead to a significantly higher Dreicer generation rate in the carbon wall case, which is less prone to be suppressed by RE loss mechanisms. The results indicate that the differences are greatly reduced above $\sim 50\%$ argon content,

suggesting that significant RE current is expected in future massive gas injection experiments on both JET and ITER.

1. Introduction

Runaway electrons (RE) with energies of several megaelectronvolts have been observed during disruptions in JET [1, 2, 3, 4, 5] and other large tokamaks. These intense electron beams are the result of the sudden cooling in connection with disruptions and may cause severe damage to the plasma facing components and vacuum vessel wall. Therefore they are considered to be a potential threat to the operation of tokamaks with high currents, such as ITER [6]. Extra care is necessary when operating with easy to melt materials, such as beryllium [7]. Understanding of the dynamics of these RE beams could help in developing methods for avoiding the beam formation or at least localized damage to the wall. Several tokamaks have studied the behaviour of these electrons during unintentional or deliberate disruptions caused for example by an intense argon or other noble gas puff [1, 2, 8]. However, proper theoretical understanding of the differences in the behaviour of runaways is still missing. One of the open questions is the different runaway behaviour in the presence of carbon and beryllium wall impurities, a question which recently gained interest in the view of the new ITER-like wall (ILW) installed at JET. The ILW comprises solid beryllium limiters and a combination of bulk tungsten and tungsten-coated carbon fibre composite divertor tiles [9].

The ILW has a significant impact on disruption physics in general [10, 11]. One of the major differences compared to disruptions with the carbon wall is that a lower fraction of energy is radiated during the disruption process, yielding higher plasma temperatures after the thermal quench. This will in turn affect the current quench times, and also the runaway beam formation. It has been observed that a slower current quench reduces the runaway generation. Drawing experimental conclusions at present time is difficult due to the limited number of runaway experiments carried out with the ILW so far. Modelling is required in order to understand the role of the different wall in the runaway behaviour and to aid the upcoming extensive runaway experiments. The aim of this paper is to perform a comparative study of two similar L-mode limiter discharges, performed with different wall materials and to provide a deeper insight in the differences. In both cases the disruption was induced by slow argon injection. We will calculate the post-disruption current profile from the plasma parameters in the two specific JET disruptive discharges, using simulations based on a one-dimensional model that solves coupled differential equations for the runaway density, heat diffusion and the plasma current in the presence of impurity injection [12].

The structure of the paper is the following. In sec. 2 we describe the scenarios that has been selected to represent typical (but similar) disruptions in JET in the presence of the carbon and beryllium wall, respectively. Here we also summarize the plasma parameters used in the simulations and the experimentally observed quantities, such

Table 1. The pre-disruption plasma parameters used in the simulations.

Parameter name	Notation	#79423 (CFC)	#81928 (ILW)
Major radius	R_0	3 m	3 m
Minor radius	a	0.88 m	0.86 m
Magnetic field on axis	B	2 T	2 T
Plasma current	I_p	1.93 MA	1.89 MA
Elongation	κ	1.3	1.3
Effective charge	Z_{eff}	$2.2 \pm 20\%$	$2.5 \pm 20\%$
Density on axis	n_0	$2.59 \cdot 10^{19} \text{ m}^{-3}$	$3.17 \cdot 10^{19} \text{ m}^{-3}$
Density profile	$n_e(r)$	$n_0(1 - 1.27 \cdot r^2)^{0.43}$	$n_0(1 - 1.32 \cdot r^2)^{0.4}$
Temperature on axis	T_0	2.17 keV	2.45 keV
Temperature profile	$T_e(r)$	$T_0(1 - 1.03 \cdot r^2)^2$	$T_0(1 - 0.98 \cdot r^2)^2$
Coulomb logarithm (on axis)	$\ln \Lambda$	23.2	22.7
q on axis	q_0	1.03	0.95
q on edge	q_a	4.05	4
q_{95}	q_{95}	3.56	3.5
q profile	$q(r/a)$	$\alpha = 1.11$	$\alpha = 1.16$
$q_0(1 - [1 - (q_0/q_a)^{1/\alpha}] \cdot (r/a)^2)^{-\alpha}$			

as runaway currents, thermal- and current quench times. Section 3 is devoted to the description of the numerical model we use for studying the runaway electron dynamics. In sec. 4 we present the results of the simulations. First we describe simulations where the temperature evolution is taken from the experiment (without modelling the impurity radiation and ionization process). Next, we include the effect of impurity injection and perform scans over the argon and background impurity (carbon or beryllium) contents that cannot be accurately determined experimentally. We calculate the plasma current evolution and radiation power and compare the simulations with experimental observations in the two cases (CFC vs ILW). Finally we assess the effect of magnetic perturbations and determine what level of perturbation is needed for runaway beam suppression. The conclusions are presented and discussed in sec. 5.

2. Scenarios selected for modelling

The two discharges selected to represent typical triggered disruption and runaway behaviour in JET are #79423 (carbon wall case) and #81928 (ILW case). These were L-mode limiter discharges, intended to be as similar as possible with respect to plasma parameters and triggering of the disruption. The basic plasma parameters are shown in table 1.

The pre-disruption density- and temperature profiles are shown in fig 1. The temperature and density profiles were obtained from Thomson scattering, right before the argon gas valve was triggered. For easier implementation we fitted typical parameter profile shape functions in the form of $A_0(1 - b \cdot r^2)^c$ to the density and temperature datasets and used the fits as the simulation input (see table 1). The fitted parameters

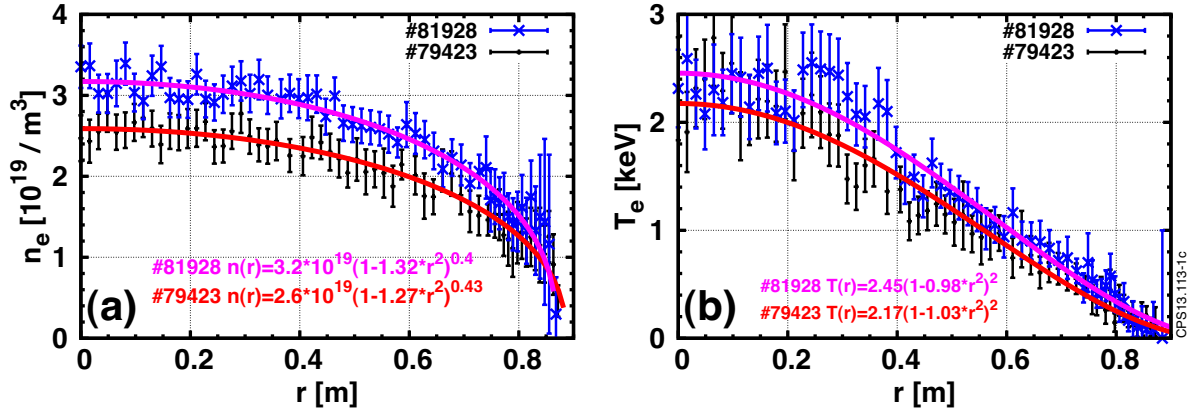


Figure 1. Typical (a) electron density- (b) electron temperature profiles for the two discharges recorded by Thomson scattering right before the argon valve trigger.

are shown with two decimal precision. Figures 1a-b contain the experimental uncertainty of the data which is also taken into account in the fits.

The disruption was triggered with a slow, controlled injection of room temperature neutral argon with a linearly increasing injection rate. The valves were triggered at 21.5 s (#79423) and 20 s (#81928). The total number of injected argon atoms was $7.39 \cdot 10^{20}$ for #79423, 30% higher than the $5.68 \cdot 10^{20}$ amount for #81928, as is shown in figure 2. The total amount of injected impurities at the time of the thermal quench is only different by $\sim 18\%$ as indicated by the vertical lines in figure 2. Note that, this stands for the *injected* material amount, the assimilation rate for the two cases is unknown.

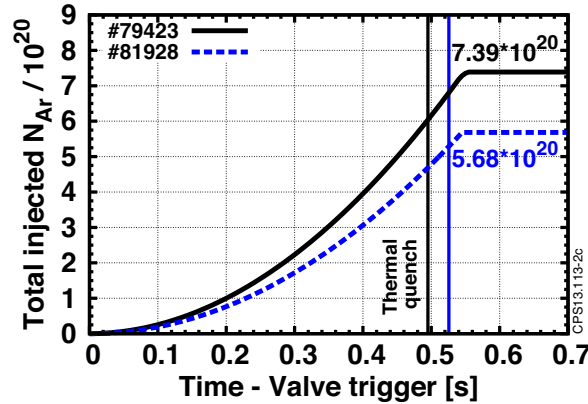


Figure 2. Total number of injected Ar atoms as a function of time. The time axis is shifted to the valve trigger time.

Figure 3a shows the evolution of the central electron temperature. Electron temperatures shown throughout the paper were obtained by the electron cyclotron emission (ECE) diagnostics. Care should be taken in the interpretation of ECE signals as during the disruption the plasma may become optically thin and suprathermal radiation

may be present in the spectrum. Also the plasma was moving upwards during the quench in shot #81928 and therefore the displayed ECE measurement does not exactly represent the core temperature 50 ms after the thermal quench. For easier comparison, the time axis is now shifted with the thermal quench (TQ) time ($t_{\text{TQ-start}} = 22.005$ s for #79423 and $t_{\text{TQ-start}} = 20.5357$ s for #81928). The thermal quench occurs at slightly different times with respect to the Ar valve trigger, although the difference of 30 ms is relatively small compared to the 500 ms delay between the valve trigger and the quench (figure 2).

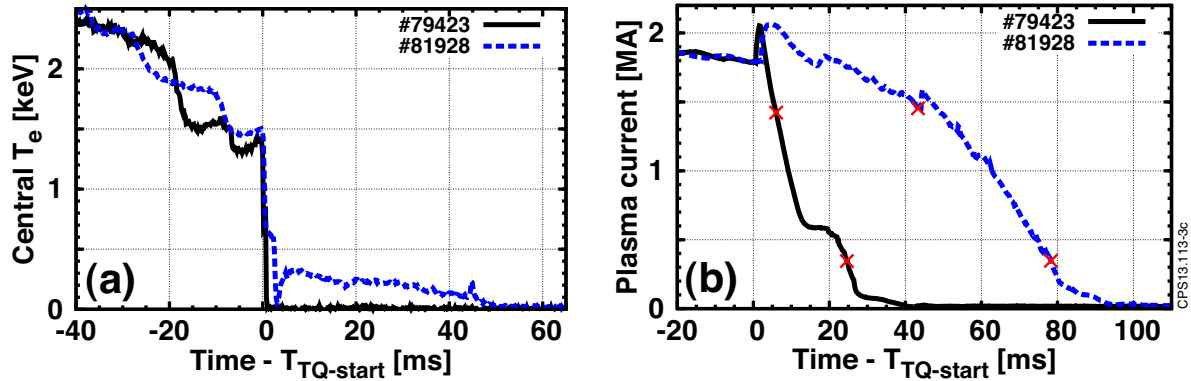


Figure 3. (a) Time evolution of the central electron temperature T_e measured by ECE. (b) Time evolution of plasma current during the current quench. Visible plateau for #79423, slow and steady drop for #81928.

A closer look in figure 3a reveals the main difference in the otherwise similar temperature collapses. Both disruptions show a relatively mild temperature decrease to ~ 1.5 keV in a 40 ms period before the TQ. In the ILW case the temperature drops down because of increased transport during the thermal quench but then it recovers up to ~ 300 eV due to the low radiation intensity and slower transport times during the current quench. The ~ 300 eV recovery is followed by a slow drop during a 50 ms timeframe. This very slow drop results in only a small amount, $\lesssim 70$ kA of runaways, as was determined by hard X-ray measurements. In the C wall case the temperature drop after 1.5 keV continues down to ~ 10 eV and gives rise to runaways with a current plateau of ~ 600 kA. Figure 3b shows the evolution of plasma current: a swift current quench with a runaway plateau at 600 kA in the C wall case, while a slow drop of current in the ILW case. The slow drop in the plasma current is not expected to generate a sufficiently high electric field for substantial runaway generation. The differences in the quench times compared to the C wall case are typical with the ILW [10]. The observed disruption- and runaway parameters are given in table 2. Red crosses in figure 3d mark the 80%/20% values used to determine the current quench (CQ) time, shown in table 2.

In the C wall case the steady state Z_{eff} is $2.2 \pm 20\%$. Although beryllium discharges in general are considered quite clean, in discharge #81928 Z_{eff} was in the $2.5 \pm 20\%$

Table 2. The disruption- and runaway parameters in the two discharges.

Parameter	#79423 (CFC)	#81928 (ILW)
Valve trigger time	21.51 s	20.01 s
Total pre-disruption plasma electrons	$8.45 \cdot 10^{20}$	$1.02 \cdot 10^{21}$
Total Ar injected	$7.39 \cdot 10^{20}$	$5.68 \cdot 10^{20}$
Ar injected up to TQ	$6 \cdot 10^{20}$	$5.07 \cdot 10^{20}$
Ar % at 100% assimilation	88%	56.8%
Thermal quench start	22.0054 s	20.5357 s
Quench delay	495.4 ms	525.7 ms
Radiated energy (in 100 ms)	~ 5.5 MJ	~ 4 MJ
CQ time (80% \rightarrow 20%)	~ 18.6 ms	~ 35.0 ms
Runaway current	~ 600 kA	< 70 kA
Runaway plateau	~ 6 ms	\emptyset

range before the thermal quench. These discharges were part of a disruption session with limiter plasmas, where the relatively low plasma density is coupled with increased wall sputtering. There is a clear exponential rise of the measured Z_{eff} in both cases during the thermal quench, but the reliability of Z_{eff} measurements during the disruption is low and values during and after the TQ have to be considered with caution.

3. Numerical model

Runaway electrons in cooling plasmas can be generated by various mechanisms: Dreicer generation [13], hot tail generation [14] and runaway avalanching [15]. The time evolution of the current density profile is determined by the runaway electron generation and the diffusion of the electric field governed by the parallel component of the induction equation

$$\frac{1}{r} \frac{\partial}{\partial r} \left(r \frac{\partial E}{\partial r} \right) = \mu_0 \frac{\partial}{\partial t} (\sigma_{\parallel} E + n_r e c), \quad (1)$$

where n_r is the number density of the runaways – travelling with approximately the speed of light – and σ_{\parallel} is the Spitzer conductivity with a neoclassical correction [16]. The changes of the (1) electric field are mainly determined by the short time scale changes of the conductivity, which strongly depends on temperature ($\sigma \propto T^{3/2}$). The model also includes a conducting plasma vessel [17, 12] but neglects coupling to the coils. In the thermal quench the conductivity drops and that induces a rising electric field which gives rise to a seed population via the Dreicer process

$$\left(\frac{dn_r}{dt} \right)_D \simeq \frac{n_e}{\tau} \left(\frac{m_e c^2}{2T_e} \right)^{3/2} \left(\frac{E_D}{E} \right)^{3(1+Z_{\text{eff}})/16} e^{-\frac{E_D}{4E} - \sqrt{\frac{(1+Z_{\text{eff}})E_D}{E}}}. \quad (2)$$

Here, $E_D = m_e^2 c^3 / (e \tau T_e)$ is the Dreicer field, and τ is the relativistic electron collision time $\tau = 4\pi \varepsilon_0^2 m_e^2 c^3 / (n_e e^4 \ln \Lambda)$ and $\ln \Lambda$ is the Coulomb logarithm. The seed runaways

are amplified via avalanching [15]:

$$\left(\frac{dn_r}{dt}\right)_{\text{avalanche}} \simeq n_r \frac{E/E_c - 1}{\tau \ln \Lambda} \sqrt{\frac{\pi\varphi}{3(Z_{\text{eff}} + 5)}} \times \left(1 - \frac{E_c}{E} + \frac{4\pi(Z_{\text{eff}} + 1)^2}{3\varphi(Z_{\text{eff}} + 5)(E^2/E_c^2 + 4/\varphi^2 - 1)}\right)^{-1/2}, \quad (3)$$

where $E_c = m_e c / (e\tau)$ is the critical electric field, $\varphi = (1 + 1.46\epsilon^{1/2} + 1.72\epsilon)^{-1}$ and $\epsilon = r/R$ denotes the inverse aspect ratio. There are several processes that can limit the energy of the runaways or contribute to their losses, such as radial diffusion due to magnetic perturbations, synchrotron radiation [18], bremsstrahlung, or plasma instabilities driven by the runaway beam anisotropy [19]. In this work, we consider losses due to radial diffusion using the Rechester-Rosenbluth diffusion estimate [20] $D_{RR} = \pi q v_{\parallel} R (\delta B/B)^2$, where $v_{\parallel} \simeq c$ is the parallel velocity, R is the major radius and $\delta B/B$ is the normalized magnetic perturbation amplitude. This numerical tool (called the GO code) was initially presented in [21, 17] and developed further in refs. [12, 22]. See reference [12] for further details and parameter scans. In the version of the GO code used in this paper, the Dreicer and avalanche runaway rates and radial losses due to magnetic field perturbations are coupled to the evolution of the electric field through equation (1). Hot tail generation is efficient if the cooling rate is comparable to the collision frequency [23] and has been predicted to be important in ITER disruptions [24], but in the cases studied in this work, the cooling times are long enough for the Dreicer generation to dominate over hot-tail generation.

The GO code requires specification of the neutral impurity density as function of time and radius, $n_{Z_i}^0(r, t)$. The time evolution is often assumed to be an exponential ramp-up, with a characteristic time on the ms timescale in agreement with numerical modelling [25]. The temperature and density evolution is modeled separately for each plasma component – electrons and Z_i ions. The energy balance equations describing the temperature evolution are

$$\begin{aligned} \frac{3}{2} \frac{\partial(n_e T_e)}{\partial t} &= \frac{3n_e}{2r} \frac{\partial}{\partial r} \left(\chi r \frac{\partial T_e}{\partial r} \right) + P_{\text{OH}} - P_{\text{line}} - P_{\text{Br}} - P_{\text{ion}} + \sum_i P_c^{eZ_i}, \quad (4) \\ \frac{3}{2} \frac{\partial(n_{Z_i} T_{Z_i})}{\partial t} &= \frac{3n_{Z_i}}{2r} \frac{\partial}{\partial r} \left(\chi r \frac{\partial T_{Z_i}}{\partial r} \right) + P_c^{Z_i e} + \sum_{j \neq i} P_c^{Z_i Z_j}. \quad (5) \end{aligned}$$

Here $P_{\text{OH}} = \sigma_{\parallel} E^2$ is the Ohmic heating power density, P_{line} and P_{Br} are the line- and Bremsstrahlung radiation and P_{ion} is the ionization energy loss. Bremsstrahlung losses are taken into account with the formula $P_{\text{Br}} = 1.69 \cdot 10^{-38} n_e^2 \sqrt{T} Z_{\text{eff}}$ [26]. Due to the different collision times the different species are modeled separately. The (5) energy balance equations are coupled with collisional energy exchange terms between Maxwellian species [27]: $P_c^{ij} = 3n_i(T_j - T_i)/2\tau_{ij}$ with the heat exchange time

$$\tau_{ij} = \frac{3\sqrt{2}\pi^{3/2}\epsilon_0^2 m_i m_j}{n_j e^4 Z_i^2 Z_j^2 \ln \Lambda} \left(\frac{T_i}{m_i} + \frac{T_j}{m_j} \right)^{3/2},$$

where the subscripts i, j now refer to electrons as well as deuterium & impurity ions. The heat diffusion coefficient is assumed to be constant ($\chi = 1 \text{ m}^2/\text{s}$) unless otherwise indicated. Studies were made in ref. [12] to test the influence of this assumption on the GO simulation results. Radiation has the strongest cooling effect on the electrons. To describe the line radiation we calculate the ionization of the impurities by calculating the density of each charge state for every ion species ($n_{Z_i}^k, k = 0..Z_i$):

$$\frac{dn_{Z_i}^k}{dt} = n_e (I_{k-1}n_{Z_i}^{k-1} - (I_k + R_k)n_{Z_i}^k + R_{k+1}n_{Z_i}^{k+1}),$$

where I_k denotes the electron impact ionization rate for the k -th charge state and R_k is the radiative recombination rate [26]. The line radiation is calculated by

$$P_{\text{line}} = \sum_i n_{Z_i} n_e L_{Z_i}(n_e, T_e).$$

The radiation rates $L_{Z_i}(n_e, T_e)$ are extracted from the ADAS database [28]. We note that from a numerical point of view this ionisation / recombination & radiation calculation is the most CPU intensive task as each transition for every charge state in every ion species has to be calculated in every time step.

4. Results and discussion

The initial plasma parameters used in the simulations are given in table 1. Apart from these, the simulations have a number of input parameters that cannot be solidly based on the experimental data, mostly due to the fact that several quantities are extremely hard to accurately determine during a disruption. Knowledge about the impurity content of the plasma, the mixing efficiency and the impurity mixing time is lacking and therefore comparison of the simulated spatio-temporal distribution of impurities is not possible. There are, however, integrated measurements available with reasonable accuracy to account for the impurity penetration, namely the evolution of plasma temperature, density, Z_{eff} or radiation. Our simulations using prescribed plasma parameter evolution show that change in plasma electron density with the experimentally measured magnitude of $\sim 30\%$ has a negligible effect on the saturation runaway current. Plasma temperature, especially its temporal evolution is more important. As will be demonstrated in this section, also Z_{eff} has a significant effect on runaway generation. Z_{eff} measurements have $\sim 20\%$ uncertainty before the disruption, and after the disruption the reliability is not good. In the following we will start with investigating the effect of the temperature evolution (setting $Z_{\text{eff}} = 1$) and in the next subsection we will model the impurity injection, including scans of argon and background impurity (carbon or beryllium) content to investigate the effect of radiation and Z_{eff} .

4.1. Prescribed temperature evolution

To determine how well the experimental measurements can be connected to the complex simulation of self-consistent current-, runaway electron-, electric field- and impurity

evolution, a somewhat simpler approach is used at first. The evolution of plasma temperature, density and Z_{eff} is prescribed and impurity evolution is not followed. This allows us to understand how these parameters affect the runaway evolution before turning to more sophisticated simulations where the evolution of the impurities determine the aforementioned quantities. $T_e(t)$ is obtained by either fitting or directly using the experimental data (with interpolation) as an input. The latter seems to be simpler and more realistic but we have to address $T_e < 0$ experimental values and the possible ambiguity of ECE T_e data. To compensate for $T_e < 0$ points and the upwards plasma movement in shot #81928 the data used 50 ms after the thermal quench is elevated based on the moving average of the experimental scatter of the recorded temperature. This correction is in the order of 10 eV in the plasma center 50 ms after the disruption and decreases gradually as the temperature decreases. In discharge #79423 the final electron temperature is in the order of 10 eV and the characteristic drop time is $\tau_0 = 0.26$ ms. Before trying to answer *why* the temperature evolution looks as it does for the two cases we wish to understand the implications of such temperature evolution on runaway electron generation.

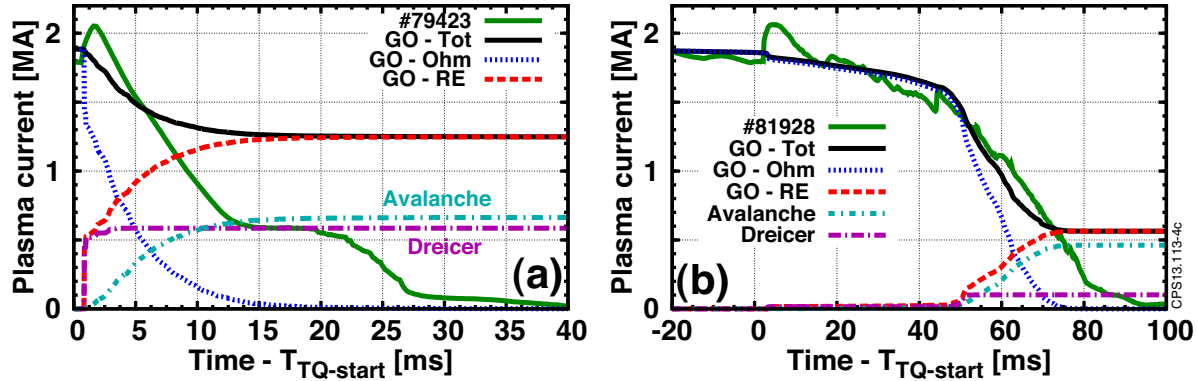


Figure 4. Evolution of different current components vs the measured plasma current evolution for (a) discharge #79423, (b) #81928. $T_e(t)$ taken from the ECE data.

First we consider the C wall case. Figure 4a shows the evolution of different current components for #79423 together with the experimental current evolution (shown with green solid line) for the case when $T_e(t)$ is taken from the ECE data. In these simulations, for simplicity Z_{eff} is set to 1. With increasing Z_{eff} the runaway current increases as will be shown later. The simulated current evolution is largely different from the experimental one. The runaway current in the discharge was $\simeq 590$ kA while in the simulated case it is 1.27 MA. One of the reasons for these differences is that at this point the evolution of plasma density, temperature and impurity profiles are not followed self-consistently. Another reason is that in the case of figure 4a-b no runaway losses are included in the numerical calculation, which would certainly be present during e.g. a violent MHD mixing scenario [25], error fields from the coils or movement towards the wall. The effect of losses due to magnetic perturbations will be assessed later in section 4.3. The

Dreicer current represents $\sim 47\%$ of the total RE current.

For the ILW case, which is shown in figure 4b, the usage of the corrected experimental temperature data leads to the generation of runaway current in the order of 4-500 kA, the majority of which generated by avalanching. This can be overcome by runaway losses as will be shown in section 4.3. If we switch off the runaway generation in the ILW case #81928 and follow the current decay due to the temperature drop including the aforementioned correction, we find a very good agreement between the simulated and the measured plasma current evolution (figure 5a). We have to note that in shot #81928 the central temperature measurement after 50 ms is highly uncertain, but with the application of the aforementioned data correction the simulated current evolution matches the experiment.

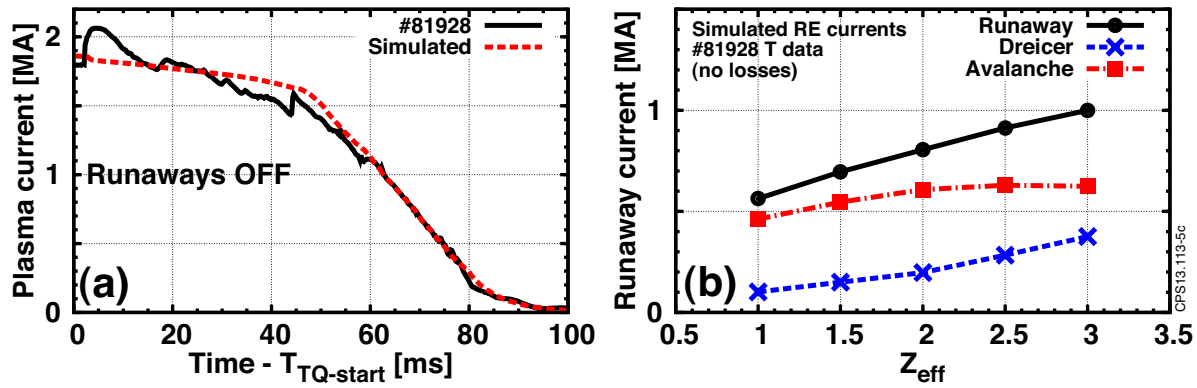


Figure 5. (a)#81928. Good agreement of simulated and experimental current evolution if runaway generation is switched off. (b) Runaway current as a function of a uniform, constant Z_{eff} in the #81928 case.

The runaway current obtained in the simulations excluding losses is too large, even in the case of $Z_{\text{eff}} = 1$. Increasing Z_{eff} will lead to even larger runaway currents. Figure 5b shows the runaway current as a function of a uniform, constant Z_{eff} with the temperature evolution of discharge #81928. The runaway current is rapidly increasing with Z_{eff} . Therefore, it is clear that more sophisticated modelling, including the effect of the injected impurities and losses are required to understand the experimental result of suppressed runaway current in the case of ILW.

4.2. Impurity injection

In this section the GO code is used in a full mode, where the evolution of plasma- and impurity parameters are calculated in a self-consistent simulation. To model the impurity radiation and ionization & recombination processes and their effect on temperature, Z_{eff} and density; the GO code requires specification of the neutral impurity density as function of time and radius. As the impurities penetrate the plasma, the energy balance equation is solved taking into account radiation, ionisation, recombination, collisions and heat diffusion [12]. This calculation determines the

temperature, Z_{eff} and density profiles, which influence the evolution of the plasma- and runaway current profiles. The evolution of the currents act back on the plasma- and impurity dynamics through Ohmic heating. In this paper, the impurity density radial profile shape is assumed to be equal to the pre-disruption electron density profile shape and its absolute value is ramped up exponentially in time to its final value with a prescribed characteristic rise time. The impurity contents are defined as the ratio of the total number of injected neutral impurity atoms to the initial total electron content (see table 2). For most of the cases we used 0.3 ms as the exponential time constant, which puts the characteristic time of the impurity evolution on the ms timescale in agreement with numerical modelling [25]. With longer impurity mixing time the quench is less energetic as the various heating mechanisms can better counteract the energy loss due to ionisation and radiation. This in turn leads to a drop in the generated runaway current, as is shown in figure 6.

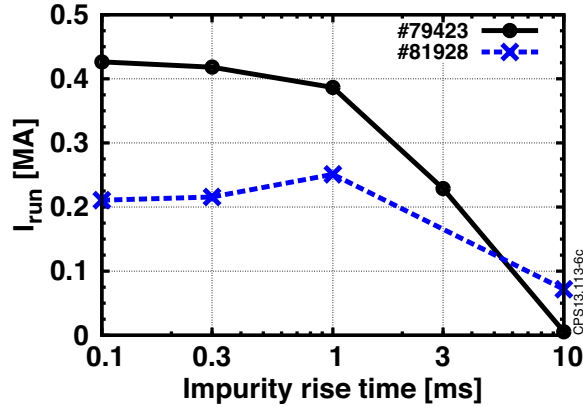


Figure 6. Runaway current for different impurity rise times with 20% Ar injected.

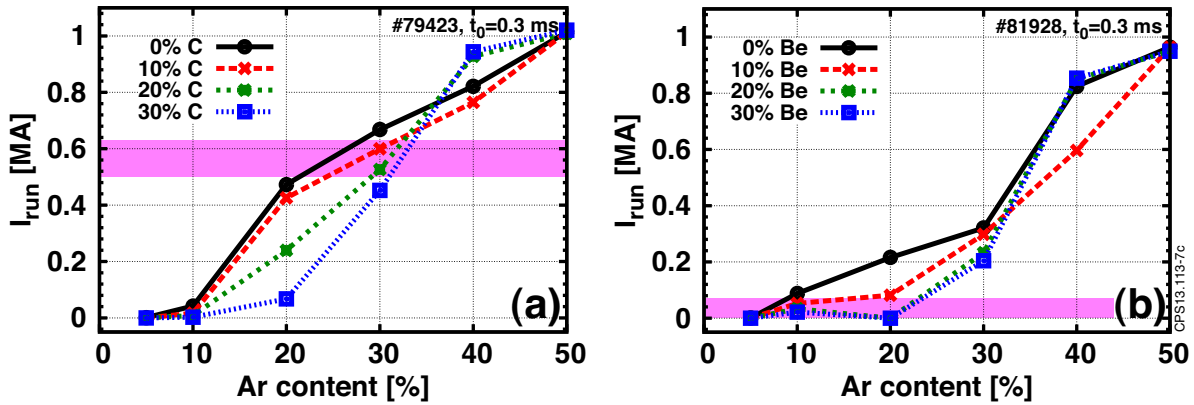


Figure 7. Runaway current for various Ar and (a) C or (b) Be contents in the representative discharges. The magenta rectangle marks the experimentally measured range of runaway current.

We have carried out scans for the argon and background impurity content to assess

the similarities or differences in the runaway behaviour in the two model discharges. The argon content can be estimated based on the total injected neutral argon amount (see table 2) with a reasonable assumption for the mixing efficiency, that is expected in the order of 30% [29, 30]. The relative amount of total argon injected in the C wall case discharge #79423 was roughly 30% more than that of discharge #81928. If we assume a similar mixing efficiency in the two cases, then the difference in the injected amount should reflect in a larger argon content of the plasma during the disruption in the C wall case. Pre-disruption Be/C levels can be estimated from the pre-disruption Z_{eff} value (table 1). However, the level of impurity sputtering during the disruption is unknown and therefore we scanned up to 30% wall impurity content.

Figure 7a shows the effect of argon and carbon content on the obtained runaway currents. As a general trend the runaway current increases with argon content, while it decreases with carbon content. The magnitude of the latter effect depends also on the argon content. The magenta rectangle represents the experimentally measured runaway current, which puts the argon content between 20-30% and the carbon content in the range of 10-30%. Note that 7% of fully ionized carbon would lead to $Z_{\text{eff}} \simeq 2.5$. 20-30% argon content is reasonable considering the injected argon amount and $\sim 30\%$ mixing. Figure 7b shows the effect of argon and beryllium. The main trend of increasing runaway current with argon content is basically the same, but the exact numbers are different. This is due to the nonlinear nature of the simulations that amplify the differences in the initial temperature- and density profiles as well as due to the presence of different background impurities. The presence of beryllium effectively reduces the runaway current at argon contents of experimental relevance ($< 20\%$). As low as 10% beryllium (corresponding to $Z_{\text{eff}} = 1.65$) leads to a factor of two decrease in runaway current. The experimentally measured $\lesssim 70$ kA runaway current is therefore reproduced at reasonable impurity contents. Comparing the 0% wall impurity cases for the same argon amounts in figures 7a-b reveals the sensitivity of runaway generation to the differences in the initial parameters. Shot #81928 shows a large reduction in the runaway current for argon contents between 5%–40%. Above 40% the runaway behaviour is similar in the two shots. This shows that the experimentally observed differences with the ILW are in part caused by the differences in plasma parameters. This effect is further enhanced by the different injected argon amount and the effect of wall impurities. The simulations indicate that the runaway current and Dreicer fraction reducing effect of the wall impurities decreases with increasing Ar content (for the plasma parameters in these shots) and the behaviour is comparable above 50% argon content. This suggests that runaway electrons may return in future experiments regardless of the ILW when argon is used in large quantities in massive gas injection (MGI) experiments on JET and ITER.

The strength of various runaway generation mechanisms also depend on the impurity contents. In figure 8a-b the two main components (Dreicer- and avalanching) are compared. As a general trend avalanching is more pronounced with increasing argon quantities. Carbon only modifies the Dreicer current fraction at $\sim 30\%$ argon

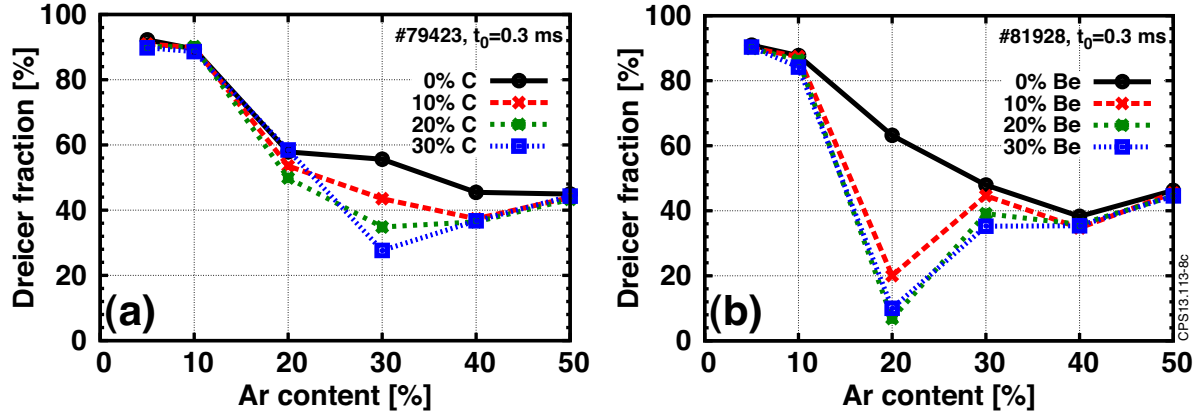


Figure 8. Dreicer current fraction for various argon and (a) carbon or (b) beryllium contents in the representative discharges. Relatively small amounts of beryllium reduce the Dreicer current fraction drastically.

content. The change in the beryllium content causes a more than 40% drop in the Dreicer contribution (and in the total runaway current) at around 20% argon content. As the growth of avalanche RE current is slower than Dreicer RE current, cases with low Dreicer fraction are more sensitive to runaway losses. This will be discussed later in section 4.3.

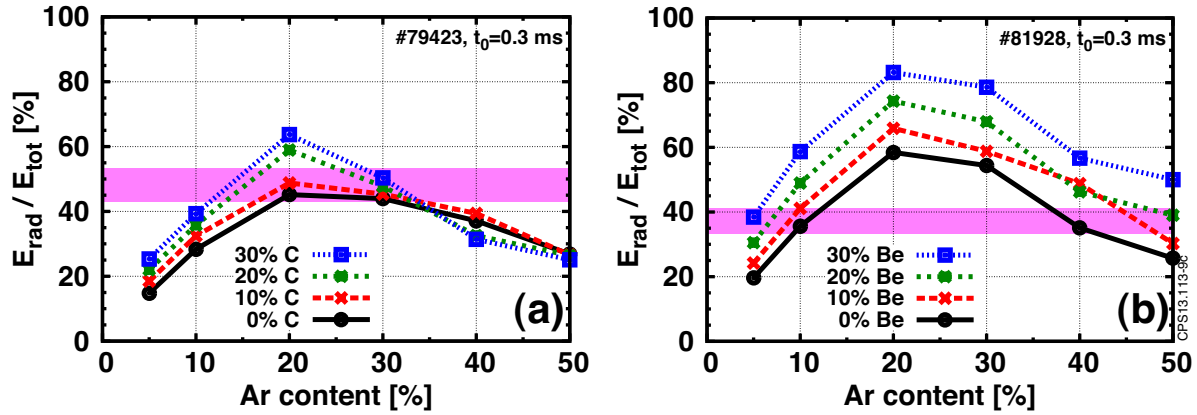


Figure 9. Total radiated energy during a 100 ms period after the thermal quench start normalized to the total plasma energy content for various argon and (a) carbon or (b) beryllium contents in the representative discharges. The magenta rectangle marks the experimentally measured total radiated energy fraction for the same period.

The radiated energy during the disruption is estimated using bolometry measurements. The radiated energy within 100 ms after the thermal quench is marked with magenta rectangles in figures 9a-b. The carbon simulations are in good agreement with the experiment in terms of radiated energy for argon content 15-30% with 10-30% carbon content. The increase in radiated energy with more carbon is not overly pronounced. The beryllium simulations show a steady, up to 50% increase in radiated

energy at higher beryllium contents. In the beryllium case the *peak* radiation power is much lower than in the carbon case, but a lower radiation level after the quench is kept until the plasma current completely decays and this sums up to a comparable order of magnitude in terms of total radiated energy in these shots. Experimental agreement is found at different Ar levels for the two shots, a lower amount of Ar is required for the ILW case. Besides the extra 30% injected argon in the carbon case of #79423, the impurity mixing can also be affected by the differences between the two shots. We have to note that comparison of the simulated and the measured plasma radiation has to be considered with caution. The total stored energy before the thermal quench is for both pulses ~ 11.4 MJ, 10.6 MJ of which is magnetic energy. Depending on the current decay, 42% (#79423) / 38% (#81928) of the magnetic energy is dissipated in the coils and structure. The maximum amount that could be radiated is therefore 58% for #79423 and 62% for #81928. The remaining energy which is not radiated or dissipated in the structure is lost by transport to the first wall. The model includes a conducting plasma structure, but not the coils, which should be implemented in future calculations along with a self-consistent handling of plasma movement towards the wall. This is expected to reduce the radiated energy and bring the simulation points closer to the measurement for the ILW case.

4.3. Diffusion losses

Magnetic perturbations can reduce the runaway electron density, as it has been shown in theoretical and numerical studies [12, 25, 31, 32, 33, 34]. Magnetic perturbations can come from the MHD mixing, error fields, instabilities enhanced by the current gradients during runaway evolution, etc. However, accurate measurement of magnetic perturbations during a disruption, especially core perturbations, is extremely challenging. In this section we will demonstrate the effect of magnetic perturbations on runaway current evolution for the two shots investigated in the paper. Figure 10a-b shows the effect of magnetic perturbations on the plasma current in the two cases, for various values of $\delta B/B$. As we are only interested in the effect of the magnetic perturbation, in these simulations, we take the temperature from the experiment, as in subsection 4.1 (and do not simulate the impurity injection itself). Without runaway losses due to magnetic perturbations, the simulation ends with a considerable runaway current in both cases, although it is higher in the C wall case (figure 10a) than in the ILW case (figure 10b). When the magnetic perturbation level is increased up to 10^{-4} , radial diffusion makes the runaway beam broader but some of the runaway current still persists. The current evolution is best matched with a perturbation level between $\delta B/B = [0.2 - 1] \times 10^{-3}$. Note, that with constant magnetic perturbation level in the simulations, we do not expect that the experimentally observed current plateau should be reproduced. In reality the magnetic perturbation level depends on time and space and therefore these simulations serve only to show the magnitude of the effect. With a perturbation level of $\delta B/B = 10^{-3}$ the runaway loss rate is comparable to the generation

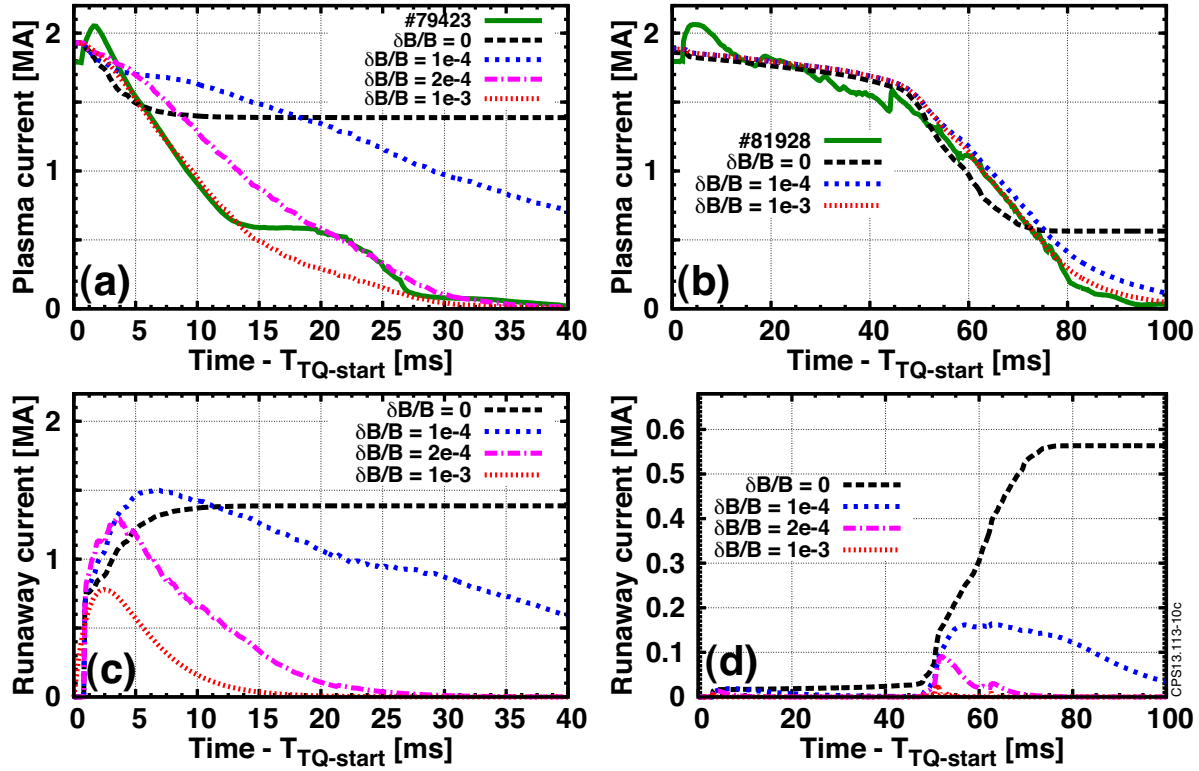


Figure 10. The effect of magnetic perturbations on plasma current evolution during disruption simulations. (a) C wall case (b) ILW case. Solid (green) lines show the measured plasma current. (c)-(d) RE current evolution corresponding to (a)-(b).

rate and the runaways spread out in the plasma before they can form a strong runaway beam. Even if the runaways are not completely removed, the runaway current density is decreased which in turn largely decreases the avalanche generation rate.

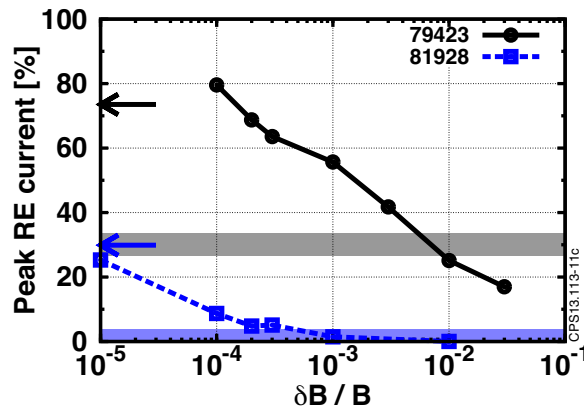


Figure 11. Peak runaway current normalized to the predischruption current as a function of $\delta B/B$ for the two cases. Arrows mark the runaway fraction corresponding to $\delta B = 0$. The grey and blue rectangles represent the experimentally measured range for the runaway current fraction.

Although the plasma current evolution is well matched in both cases at the same level of magnetic perturbation, the fraction of runaway current is different in the two cases, just as was observed in the experiments. Figures 10c-d show that the runaway current ramps up with time roughly as $1 - \exp(-t/\tau_g)$, where τ_g is the loss time. If a $\delta B > 0$ perturbation is present it also drops exponentially, but with a different τ_l loss time constant. Figure 11 shows the *peak* runaway current normalized to the predischruption current as a function of $\delta B/B$ for the two different shots. As a comparison, grey and blue rectangles show the experimentally measured range for the runaway current fraction as measured in the *plateau*. Arrows mark the runaway fraction corresponding to $\delta B = 0$ in the simulations (note the logarithmic δB axis) which is $\sim 73\%$ for the C wall case and $\sim 30\%$ for the ILW case. The maximum value of the runaway current drops exponentially as a function of δB . Note that even relatively high RE currents can be dropped to practically zero within a few tens of milliseconds if the perturbation level is $\delta B/B > 2 \times 10^{-4}$ (figure 10c-d). The reduction is larger in shot #81928 than in #79423. The reason why the ILW case is more sensitive to the losses due to magnetic perturbations than the C wall case is that in the C wall case the Dreicer mechanism is significantly stronger (figure 4a), generating a higher fraction of the runaway current than in the ILW case (figure 4b). The Dreicer generation has approximately an order of magnitude shorter characteristic rise time than the avalanche mechanism, and therefore the losses due to radial diffusion can more easily counteract the runaway growth if the Dreicer current fraction is low. The impurity injection simulations have shown that not only the runaway current but also the Dreicer fraction is significantly lower for experimentally relevant argon and wall impurity contents with the ILW (see figures 7 and 8.) Figure 11 shows that not only the time evolution of the plasma current but also the order of magnitude of the runaway current fraction is well matched with the experiments at the similar level of magnetic perturbations, $\delta B/B > 2 \times 10^{-4}$.

5. Discussion and conclusions

As accurate knowledge about the realistic impurity levels is not available, comparison between simulations and experiments need to be based on reasonable assumptions about impurity content and rise time. Our analysis focuses on the effect of temperature evolution, impurity contents and magnetic perturbation levels on runaway electron dynamics and current evolution. In general, the results of the numerical simulations are in reasonable agreement with the experimental observations. The best agreement between simulation and experimental observation in terms of current, radiation and temperature evolution are reached at $\gtrsim 10\%$ background impurity content, which is reasonable considering the relatively high Z_{eff} even before argon injection. In terms of argon content the best agreement is found in the 20-30% range that aligns well with the injected argon amounts at $\sim 30\%$ mixing.

Our results show that the differences between the C wall and ILW cases are due to

(1) the difference in the initial parameters, (2) the difference in the injected/mixed argon amount, and (3) the different radiation characteristics of beryllium and carbon. Since these three main differences between the discharges have a positive feedback in terms of runaway generation, the effects of differences in the plasma parameters and injected argon amount are enhanced by the presence of different wall (carbon or beryllium) impurities. Although the discharges were selected to be similar, in the ILW case both the initial electron temperature and density are higher, which are exposed to a lower amount of injected argon.

This modelling shows that variations in the argon content in these shots have a considerable effect on the runaway generation. The Dreicer fraction is reduced by the presence of beryllium, but is almost unaffected by the presence of carbon (at the same argon content). This results in a lower Dreicer current generation in the ILW case compared with the C wall case. The runaway population in the ILW case consists mostly of slowly growing avalanche runaways and they are effectively transported out from the plasma by a low level of magnetic perturbations or other losses. Note, that the presence of beryllium is beneficial only if the amount of argon is not too large. In our simulations the combination of 20% argon and 10% beryllium content effectively reduced the Dreicer fraction of the runaway current. Above 40-50% argon content the differences due to plasma parameters and wall material are reduced and eventually vanish. In view of the results of this paper, upcoming massive gas injection experiments with the ILW will most probably have to face with the reoccurrence of runaways for the scenarios that produced runaways using MGI with the carbon wall. Dedicated runaway experiments with the ILW on JET are necessary to be able to better estimate the runaway behaviour in ITER.

Further improvement of the numerical model would be to take into account the spatio-temporal dependence of heat conductivity χ_e and the plasma movement towards the wall. Direct removal of runaways via first wall scrape off is not expected in these cases, since the runaway current channel width is smaller in the simulations than the distance of the magnetic axis from the first wall in the corresponding time instants of the discharges. However, the wall itself can contribute to the removal of plasma current and energy as well as changes in the plasma inductance and thus may influence the evolution of the other parameters.

Acknowledgments

This research was funded partly by the European Communities under the contract of Association between EURATOM and *Vetenskapsrådet* and was carried out within the framework of the European Fusion Development Agreement. The views and opinions expressed herein do not necessarily reflect those of the European Commission. The authors are grateful to C. Sozzi, D. Réfy, E. Delabie, M. Stamp, A. Boboc, G. Pokol and L. Capone for fruitful discussions.

References

- [1] J.A. Wesson, R.D. Gill, M. Hugon, F.C. Schüller, J.A. Snipes, D.J. Ward, D.V. Bartlett, D.J. Campbell, P.A. Duperrex, A.W. Edwards, R.S. Granetz, N.A.O. Gottardi, T.C. Hender, E. Lazzaro, P.J. Lomas, N. Lopes Cardozo, K.F. Mast, M.F.F. Nave, N.A. Salmon, P. Smeulders, P.R. Thomas, B.J.D. Tubbing, M.F. Turner, and A. Weller. Disruptions in JET. *Nuclear Fusion*, 29(4):641. <http://stacks.iop.org/0029-5515/29/i=4/a=009>.
- [2] R.D. Gill. Generation and loss of runaway electrons following disruptions in JET. *Nuclear Fusion*, 33(11):1613, 1993. <http://stacks.iop.org/0029-5515/33/i=11/a=I03>.
- [3] R.D. Gill, B. Alper, M. de Baar, T.C. Hender, M.F. Johnson, V. Riccardo, and contributors to the EFDA-JET Workprogramme. Behaviour of disruption generated runaways in jet. *Nuclear Fusion*, 42(8):1039, 2002. <http://stacks.iop.org/0029-5515/42/i=8/a=312>.
- [4] V. Riccardo and JET EFDA contributors. Disruptions and disruption mitigation. *Plasma Physics and Controlled Fusion*, 45(12A):A269, 2003. <http://stacks.iop.org/0741-3335/45/i=12A/a=018>.
- [5] V.V. Plyusnin, V. Riccardo, R. Jaspers, B. Alper, V.G. Kiptily, J. Mlynar, S. Popovichev, E. de La Luna, F. Andersson, and JET EFDA contributors. Study of runaway electron generation during major disruptions in JET. *Nuclear Fusion*, 46(2):277, 2006. <http://stacks.iop.org/0029-5515/46/i=2/a=011>.
- [6] T.C. Hender, J.C. Wesley, J. Bialek, A. Bondeson, A.H. Boozer, R.J. Buttery, A. Garofalo, T.P. Goodman, R.S. Granetz, Y. Gribov, O. Gruber, M. Gryaznevich, G. Giruzzi, S. GÄijnter, N. Hayashi, P. Helander, C.C. Hegna, D.F. Howell, D.A. Humphreys, G.T.A. Huysmans, A.W. Hyatt, A. Isayama, S.C. Jardin, Y. Kawano, A. Kellman, C. Kessel, H.R. Koslowski, R.J. La Haye, E. Lazzaro, Y.Q. Liu, V. Lukash, J. Manickam, S. Medvedev, V. Mertens, S.V. Mirnov, Y. Nakamura, G. Navratil, M. Okabayashi, T. Ozeki, R. Paccagnella, G. Pautasso, F. Porcelli, V.D. Pustovitov, V. Riccardo, M. Sato, O. Sauter, M.J. Schaffer, M. Shimada, P. Sonato, E.J. Strait, M. Sugihara, M. Takechi, A.D. Turnbull, E. Westerhof, D.G. Whyte, R. Yoshino, H. Zohm, Disruption the ITPA MHD, and Magnetic Control Topical Group. Progress in the ITER physics basis chapter 3: MHD stability, operational limits and disruptions. *Nuclear Fusion*, 47(6):S128–S202, 2007. <http://stacks.iop.org/0029-5515/47/i=6/a=S03>.
- [7] B. Bazylev, G. Arnoux, S. Brezinsek, Yu. Igitchanov, M. Lehnen, V. Riccardo, and V. Kiptily. Modeling of the impact of runaway electrons on the ILW in JET. *Journal of Nuclear Materials*, 438, Supplement(0):S237 – S240, 2013.
- [8] M. Lehnen, A. Alonso, G. Arnoux, N. Baumgarten, S.A. Bozhnikov, S. Brezinsek, M. Brix, T. Eich, S.N. Gerasimov, A. Huber, S. Jachmich, U. Kruezi, P.D. Morgan, V.V. Plyusnin, C. Reux, V. Riccardo, G. Sergienko, M.F. Stamp, and JET EFDA contributors. Disruption mitigation by massive gas injection in jet. *Nuclear Fusion*, 51(12):123010, 2011. <http://stacks.iop.org/0029-5515/51/i=12/a=123010>.
- [9] G. F. Matthews, M. Beurskens, S. Brezinsek, M. Groth, E. Joffrin, A. Loving, M. Kear, M-L Mayoral, R. Neu, P. Prior, V. Riccardo, F. Rimini, M. Rubel, G. Sips, E. Villedieu, P. de Vries, M. L. Watkins, and EFDA-JET contributors. JET ITER-like wall—overview and experimental programme. *Physica Scripta*, 2011(T145):014001, 2011. <http://stacks.iop.org/1402-4896/2011/i=T145/a=014001>.
- [10] P. C. de Vries, G. Arnoux, A. Huber, J. Flanagan, M. Lehnen, V. Riccardo, C. Reux, S. Jachmich, C. Lowry, G. Calabro, D. Frigione, M. Tsalas, N. Hartmann, S. Brezinsek, M. Clever, D. Douai, M. Groth, T. C. Hender, E. Hodille, E. Joffrin, U. Kruezi, G. F. Matthews, J. Morris, R. Neu, V. Philipps, G. Sergienko, M. Sertoli, and JET EFDA contributors. The impact of the ITER-like wall at JET on disruptions. *Plasma Physics and Controlled Fusion*, 54(12):124032, 2012. <http://stacks.iop.org/0741-3335/54/i=12/a=124032>.
- [11] M. Lehnen, G. Arnoux, N. Hartmann, S. Brezinsek, S. Devaux, A. Huber, S. Jachmich, U. Kruezi, G.F. Matthews, C. Reux, V. Riccardo, B. Sieglin, M.F. Stamp,

- and P.C. de Vries. Disruption heat loads and their mitigation in JET with the ITER-like wall. *Journal of Nuclear Materials*, 2013. (Corrected proof) <http://www.sciencedirect.com/science/article/pii/S002231151300024X>.
- [12] T. Fehér, H. M. Smith, T. Fülöp, and K. Gál. Simulation of runaway electron generation during plasma shutdown by impurity injection in ITER. *Plasma Physics and Controlled Fusion*, 53(3):035014, 2011. <http://stacks.iop.org/0741-3335/53/i=3/a=035014>.
- [13] J.W. Connor and R.J. Hastie. Relativistic limitations on runaway electrons. *Nuclear Fusion*, 15(3):415, 1975. <http://stacks.iop.org/0029-5515/15/i=3/a=007>.
- [14] R. W. Harvey, V. S. Chan, S. C. Chiu, T. E. Evans, M. N. Rosenbluth, and D. G. Whyte. Runaway electron production in DIII-D killer pellet experiments, calculated with the CQL3D/KPRAD model. *Physics of Plasmas*, 7(11):4590–4599, 2000. <http://link.aip.org/link/?PHP/7/4590/1>.
- [15] M.N. Rosenbluth and S.V. Putvinski. Theory for avalanche of runaway electrons in tokamaks. *Nuclear Fusion*, 37(10):1355, 1997. <http://stacks.iop.org/0029-5515/37/i=10/a=I03>.
- [16] John Wesson. *Tokamaks*. Clarendon Press, Oxford, third edition, 2004. <http://www.iop.org/EJ/abstract/0741-3335/46/3/173515>.
- [17] H. Smith, P. Helander, L.-G. Eriksson, D. Anderson, M. Lisak, and F. Andersson. Runaway electrons and the evolution of the plasma current in tokamak disruptions. *Physics of Plasmas*, 13(10):102502, 2006. <http://link.aip.org/link/?PHP/13/102502/1>.
- [18] F. Andersson, P. Helander, and L.-G. Eriksson. Damping of relativistic electron beams by synchrotron radiation. *Physics of Plasmas*, 8(12):5221–5229, 2001. <http://link.aip.org/link/?PHP/8/5221/1>.
- [19] T. Fülöp, H. M. Smith, and G. Pokol. Magnetic field threshold for runaway generation in tokamak disruptions. *Physics of Plasmas*, 16(2):022502, 2009. <http://link.aip.org/link/?PHP/16/022502/1>.
- [20] A. B. Rechester and M. N. Rosenbluth. Electron heat transport in a tokamak with destroyed magnetic surfaces. *Phys. Rev. Lett.*, 40(1):38–41, Jan 1978. http://prl.aps.org/abstract/PRL/v40/i1/p38_1.
- [21] L.-G. Eriksson, P. Helander, F. Andersson, D. Anderson, and M. Lisak. Current dynamics during disruptions in large tokamaks. *Phys. Rev. Lett.*, 92(20):205004, May 2004. <http://prl.aps.org/abstract/PRL/v92/i20/e205004>.
- [22] K Gál, T Fehér, H Smith, T Fülöp, and P Helander. Runaway electron generation during plasma shutdown by killer pellet injection. *Plasma Physics and Controlled Fusion*, 50(5):055006, 2008. <http://stacks.iop.org/0741-3335/50/i=5/a=055006>.
- [23] P. Helander, H. Smith, T. Fülöp, and L.-G. Eriksson. Electron kinetics in a cooling plasma. *Physics of Plasmas*, 11(12):5704–5709, 2004. <http://link.aip.org/link/?PHP/11/5704/1>.
- [24] H. Smith, P. Helander, L.-G. Eriksson, and T. Fülöp. Runaway electron generation in a cooling plasma. *Physics of Plasmas*, 12(12):122505, 2005. <http://link.aip.org/link/?PHP/12/122505/1>.
- [25] V.A. Izzo, E.M. Hollmann, A.N. James, J.H. Yu, D.A. Humphreys, L.L. Lao, P.B. Parks, P.E. Sieck, J.C. Wesley, R.S. Granetz, G.M. Olynky, and D.G. Whyte. Runaway electron confinement modelling for rapid shutdown scenarios in DIII-D, Alcator C-Mod and ITER. *Nuclear Fusion*, 51(6):063032, 2011. <http://stacks.iop.org/0029-5515/51/i=6/a=063032>.
- [26] J. D. Huba. *NRL Plasma Formulary*. Number NRL/PU/6790–00-426. Naval Research Laboratory, Washington DC, revised edition, 2006. <http://wwwppd.nrl.navy.mil/nrlformulary/>.
- [27] P. Helander and D. J. Sigmar. *Collisional transport of magnetized plasmas*. Cambridge University Press, Cambridge, 2002.
- [28] H. P. Summers. *The ADAS User Manual, version 2.6*, 2004. <http://www.adas.ac.uk/manual.php>.
- [29] E.M. Hollmann, T.C. Jernigan, P.B. Parks, J.A. Boedo, T.E. Evans, M. Groth, D.A. Humphreys, A.N. James, M.J. Lanctot, D. Nishijima, D.L. Rudakov, H.A. Scott, E.J. Strait, M.A. Van

- Zeeland, J.C. Wesley, W.P. West, W. Wu, and J.H. Yu. Measurements of injected impurity assimilation during massive gas injection experiments in DIII-D. *Nuclear Fusion*, 48(11):115007, 2008. <http://stacks.iop.org/0029-5515/48/i=11/a=115007>.
- [30] C. Reux. Private communication, 2013.02.06.
- [31] P. Helander, L.-G. Eriksson, and F. Andersson. Suppression of runaway electron avalanches by radial diffusion. *Physics of Plasmas*, 7(10):4106–4111, 2000. <http://link.aip.org/link/?PHP/7/4106/1>.
- [32] G. Papp, M. Drevlak, T. Fülöp, and P. Helander. Runaway electron drift orbits in magnetostatic perturbed fields. *Nuclear Fusion*, 51(4):043004, 2011. <http://iopscience.iop.org/0029-5515/51/4/043004>.
- [33] G. Papp, M. Drevlak, T. Fülöp, P. Helander, and G. I. Pokol. Runaway electron losses caused by resonant magnetic perturbations in ITER. *Plasma Physics and Controlled Fusion*, 53(9):095004, 2011. <http://stacks.iop.org/PPCF/53/095004>.
- [34] G Papp, M Drevlak, T Fülöp, and G I Pokol. The effect of resonant magnetic perturbations on runaway electron transport in iter. *Plasma Physics and Controlled Fusion*, 54(12):125008, 2012. <http://stacks.iop.org/0741-3335/54/i=12/a=125008>.